JOURNAL OF RAW MATERIALS ENGINEERING

2026, vol. 1, iss. 1, pp. 37–60

https://doi.org/10.7494/jrme.2026.1.1.8604

Satellite-enabled decision support for reservoir water availability, flood dynamics, and catchment stress in semi-arid regions

Thatikonda Naresh[1]*, Sandeep Bandipally[1], Ashok Amgoth[2], Matta Keshava Reddy[1], Shaik Saleemmiya[1]

[1] Department of Civil Engineering, ACE Engineering College, Hyderabad 501301, Telangana, India
[2] Department of Civil Engineering, Prasad V. Potluri Siddhartha Institute of Technology, Vijayawada 520007, Andhra Pradesh, India
* Corresponding author

Authors' e-mails: naresh.phd20@nitap.ac.in, sandeep.bandipally@aceec.ac.in, ashok@pvpsiddhartha.ac.in, mettakeshav@gmail.com, s.saleemmiya@aceec.ac.in

Abstract: Sustainable operation of inland reservoirs in semi-arid regions is increasingly challenged by intensified hydro-climatic variability and rapid catchment-scale land-use transformation, leading to increased flood risk and seasonal water stress. This study develops a satellite-enabled decision-support framework for assessing reservoir water availability, flood dynamics, and catchment-induced hydrological stress, using Pakhal Lake, Telangana, India, as a representative case study. Temporally smoothed Sentinel-2-derived vegetation and water indices were used to evaluate seasonal and interannual variability in reservoir conditions, while cloud-independent Sentinel-1 SAR imagery enabled reliable delineation of flood inundation during extreme monsoon events. Catchment land-use dynamics were quantified using machine-learning classifiers within the Google Earth Engine platform to identify anthropogenic pressures affecting reservoir inflows and storage behaviour. Results reveal pronounced seasonal variability in reservoir water extent and vegetation condition, with SAR analysis indicating an approximately 28% expansion of inundated area during the extreme monsoon year of 2018. Rapid growth of built-up and bare land within the catchment indicates increasing hydrological stress with implications for runoff generation and reservoir sustainability. The proposed framework provides actionable indicators for reservoir operation, irrigation planning, and flood preparedness, offering a scalable and cost-effective monitoring approach for water resource management in data-scarce semi-arid regions.

Keywords: reservoir operation, water availability, flood risk management, catchment land-use change, decision-support systems, semi-arid water resources

Received: 2.04.2026
Accepted: 25.05.2026
Published: 27.07.2026

1. Introduction

Inland reservoirs are critical water resources infrastructure in semi-arid and monsoon-dominated regions, where they regulate seasonal runoff, support irrigation and domestic supply, mitigate floods, and sustain regional economic activity (Mitsch et al., 2023). In countries such as India, reservoirs and traditional tank systems form the backbone of agricultural productivity and groundwater recharge, particularly in water-scarce landscapes characterised by strong interannual rainfall variability (Bassi et al., 2014; Davidson, 2014; Mohanty et al., 2020; Priyadarshini, 2025). The reliable operation of these systems is increasingly challenged by intensified hydro-climatic variability and rapid catchment-scale land-use changes, which together alter inflow regimes, storage behaviour, flood response, and long-term water availability.

Recent decades have seen an increase in extreme rainfall events alongside prolonged dry spells across many semi-arid regions, amplifying both flood risk during monsoon periods and water stress during dry seasons (Jain et al., 2020; Sheffield et al., 2012). These changes place reservoirs under competing operational demands, requiring simultaneous flood attenuation and water-supply reliability. At the same time, accelerated urbanisation, agricultural intensification, infrastructure expansion, and land degradation within reservoir catchments have modified runoff generation processes, increased sediment delivery, and reduced effective storage capacity (Bassi et al., 2014; Shekar & Mathew, 2023). The combined influence of climatic and anthropogenic pressures has transformed many reservoirs into increasingly sensitive and operationally constrained systems.

From a water-resources and industry perspective, inland reservoirs in India and other semi-arid regions function not only as storage assets but also as critical flood-moderation infrastructure during high-intensity monsoon rainfall (Mohanty et al., 2020). Unregulated catchment development and inadequate land-use controls have compromised this flood-buffering function, resulting in higher peak inflows, increased stress on spillway operations, and elevated downstream flood risk. Simultaneously, excessive abstraction and sedimentation reduce dry-season storage reliability, exacerbating irrigation shortages and increasing dependence on groundwater during delayed or deficient monsoon years (Shekar & Mathew, 2023). These challenges underscore the need for operational monitoring tools that can support adaptive reservoir management under evolving hydro-climatic and land-use conditions.

Effective reservoir operation requires continuous, spatially explicit information on water availability, flood extent, vegetation condition, and catchment land-use dynamics. However, conventional monitoring approaches based on in situ gauges, periodic surveys, and field inspections are often constrained by sparse spatial coverage, inconsistent data availability, and delayed reporting, particularly in data-scarce regions of the Global South (Mohanty et al., 2020). As a result, reservoir operators frequently rely on reactive decision-making, limiting their ability to anticipate flood hazards, optimise storage allocation, or manage seasonal water stress proactively.

Satellite remote sensing offers a scalable and cost-effective means of addressing these limitations by enabling systematic observation of surface-water dynamics, vegetation response, and catchment conditions over large spatial and temporal scales (Hu et al., 2017). Optical indices such as the normalised difference vegetation index (NDVI) and the normalised difference water index (NDWI) are widely used to monitor vegetation condition and surface-water extent, providing indirect and direct indicators of reservoir water availability relevant to irrigation planning and seasonal storage assessment (Barbosa et al., 2006; McFeeters, 1996; Peng K. et al., 2025). However, the operational use of optical data in monsoon-dominated regions is constrained by persistent cloud cover and atmospheric noise, necessitating robust temporal smoothing and gap-filling approaches to ensure reliable decision-support outputs (Fu et al., 2024; Kumari et al., 2021).

Cloud-independent synthetic aperture radar (SAR) data provide a complementary capability for flood monitoring under adverse weather conditions, enabling reliable delineation of inundation extent during extreme monsoon events (Lang et al., 2024; Narin et al., 2025). When combined with machine-learning-based land-use analysis, satellite observations can also quantify catchment transformations that directly influence runoff generation, sediment delivery, and reservoir stress (Belgiu & Drăguț, 2016; Shekar & Mathew, 2023).

Despite these advances, the operational uptake of satellite-based monitoring for reservoir management remains limited. Many studies emphasise land-cover classification or ecological assessment without explicitly translating satellite-derived indicators into information usable for reservoir operation, flood preparedness, or water-allocation planning (Merchant et al., 2023; Mohanty et al., 2020). Moreover, integrated frameworks that combine temporally smoothed optical indices, SAR-based flood mapping, and machine-learning-derived catchment indicators within a single operational decision-support system remain underdeveloped, particularly for small to medium inland reservoirs in semi-arid India.

Many previous studies have focused primarily on either ecological wetland mapping, isolated flood detection, or static land-cover assessment without integrating these components into an operational reservoir-management framework. Additionally, limited attention has been given to linking satellite-derived indicators directly with reservoir operation, flood preparedness, and catchment-induced hydrological stress. The present study addresses these limitations by integrating temporally smoothed optical indices, SAR-based flood mapping, and machine-learning-based catchment analysis into a unified decision-support framework specifically designed for semi-arid reservoir systems. Pakhal Lake provides an appropriate case study for evaluating the applicability of this integrated framework under conditions of increasing hydro-climatic and catchment stress.

Pakhal Lake, a historic inland reservoir in Telangana, India, exemplifies these challenges. The reservoir supports irrigation, fisheries, and groundwater recharge while functioning as a flood-buffering system during extreme monsoon events. In recent decades, Pakhal Lake has experienced accelerated catchment transformation, sediment exposure, and heightened hydro-climatic variability, making it a representative system for assessing operational stress in semi-arid reservoirs (Shekar & Mathew, 2023).

In this context, the present study applies the proposed integrated satellite-based framework to evaluate the reservoir water availability, flood dynamics, and catchment-induced hydrological stress in Pakhal Lake, Telangana. Using multi-sensor satellite observations and machine-learning analysis within the Google Earth Engine platform, the study aims to generate operationally relevant indicators that support reservoir management, flood preparedness, and sustainable water-resources planning in semi-arid regions.

2. Materials and methods

2.1. Study area

Pakhal Lake is a historic inland freshwater reservoir located in the Warangal district of Telangana State, India, between latitudes 17°56′–17°59′ N and longitudes 79°56′–79°59′ E, at an average elevation of approximately 520 m above mean sea level (Aquino et al., 2024; Shekar & Mathew, 2023). The study area is shown in Fig. 1. The lake was constructed during the Kakatiya dynasty in 1213 AD by impounding Munneru Vagu, a tributary of the Godavari River basin. Pakhal Lake serves as a critical source of irrigation water, groundwater recharge, and a habitat for fisheries, as well as migratory and resident species.

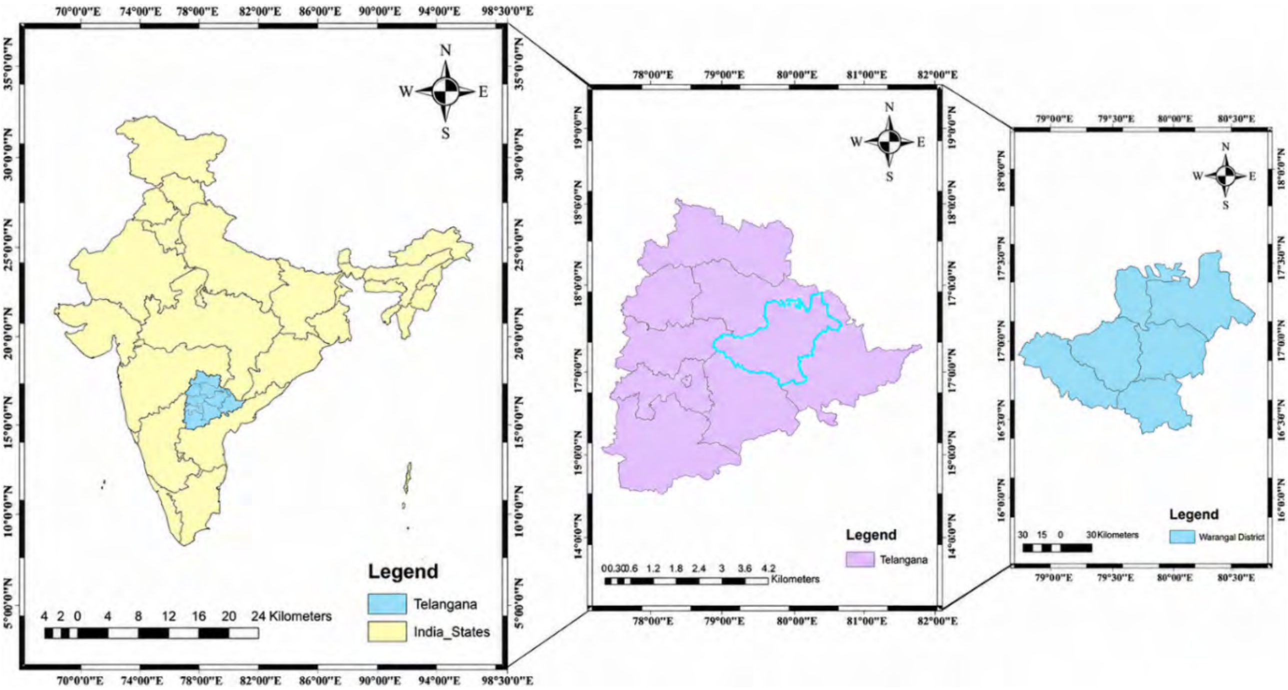

Fig. 1. Location of the Pakhal Lake study area in Warangal District, Telangana, India

The lake is situated in a catchment area of approximately 270 km², characterised by undulating topography, lateritic and red soils, mixed deciduous forest patches, agricultural lands, and rapidly expanding peri-urban settlements (Shekar & Mathew, 2023). The regional climate is classified as tropical semi-arid with a mean annual rainfall of nearly 900 mm, of which over 85% is received during the southwest monsoon period (June–October) (India Meteorological Department, 2020). Seasonal air temperatures range from 18°C in winter to above 42°C in summer, resulting in strong evapotranspiration-driven water-level fluctuations (Aquino et al., 2024). In recent decades, the lake has undergone accelerated land-use transformation, sediment deposition, urban encroachment, and intensifying hydro-climatic extremes, making it an ideal test site for long-term wetland monitoring.

2.2. Satellite data and ancillary datasets

A multi-sensor satellite dataset integrating optical, radar, and topographic information was used to characterise the hydro-ecological dynamics of Pakhal Lake for the period 2016–2021. All datasets were accessed, processed, and analysed within the Google Earth Engine (GEE) cloud-computing environment (Gorelick et al., 2017). The details of all satellite and ancillary datasets used in this study are presented in Tab. 1.

Tab. 1. Multi-sensor satellite datasets and ancillary data utilised for spatio-temporal wetland analysis of Pakhal Lake (2016–2021)

Dataset	Sensor/platform	Spatial resolution	Temporal coverage	Spectral bands used	Purpose/application	Data source (GEE ID)
Sentinel-2 MSI	Copernicus/ESA	10 m (VIS–NIR), 20 m (SWIR)	2016–2021	B2 (Blue), B3 (Green), B4 (Red), B8 (NIR)	NDVI & NDWI computation, LULC classification	COPERNICUS/S2_SR
Landsat-8 OLI/TIRS	NASA–USGS	30 m	2018–2020	B4 (Red), B5 (NIR), B6 (SWIR1)	temporal comparison & validation	LANDSAT/LC08/C01/T1_TOA
SRTM DEM	NASA/USGS	30 m	2016	topographic correction & flood mapping	USGS/SRTMGL1_003	USGS/SRTMGL1_003
Ground reference	Google Earth & field survey	~1 m	2019–2020	visual interpretation points	accuracy assessment	–

2.2.1. Sentinel-2 MSI

Sentinel-2 Level-2A surface reflectance products were used as the primary data source for vegetation, water index computation, and land-use/land-cover (LULC) classification. The sensor provides multispectral imagery at spatial resolutions of 10 m (for visible and near-infrared bands), 20 m (for red-edge and shortwave infrared bands), and 60 m (for atmospheric correction bands), with a revisit time of 5 days (Kumari et al., 2021; Merchant et al., 2023). Bands B2 (Blue), B3 (Green), B4 (Red), and B8 (NIR) were used for NDVI and NDWI computation, as well as LULC feature extraction.

2.2.2. Sentinel-1 SAR

Sentinel-1 C-band synthetic aperture radar (SAR) ground range detected (GRD) products acquired in interferometric wide (IW) mode with vertical transmit–horizontal receive (VH) polarisation were used for cloud-independent flood inundation mapping (Lang et al., 2024; Narin et al., 2025). The spatial resolution is 10 m with a revisit time of 6–12 days.

2.2.3. Landsat-8 OLI/TIRS

Landsat-8 imagery (30 m spatial resolution) was utilised for long-term contextual validation of water and vegetation patterns over the selected period (2018–2020).

2.2.4. Digital elevation model and ground reference data

A 30 m resolution Shuttle Radar Topography Mission (SRTM) digital elevation model (DEM) was used for slope-based flood masking and topographic correction. Ground reference data for classification accuracy assessment were derived from high-resolution Google Earth imagery and limited field surveys conducted between 2019 and 2020.

2.3. Image preprocessing and atmospheric correction

All satellite data were preprocessed using standardised workflows implemented in GEE. Sentinel-2 Level-2A data, atmospherically corrected using the Sen2Cor processor, were directly used as bottom-of-atmosphere surface reflectance products (Louis et al., 2016). Cloud and shadow contamination were removed using a combined approach based on the QA60 bitmask and the s2cloudless probabilistic cloud detection algorithm with a strict cloud probability threshold of 10% (Kumari et al., 2021; Narin et al., 2025).

All images were reprojected to the WGS 84 / UTM Zone 44N coordinate system. Radiometric normalisation was applied to ensure cross-temporal comparability. To minimise atmospheric noise and reduce cloud artefacts, monthly median composites were generated, followed by annual median composites for the period 2016–2021 (Merchant et al., 2023; Pan et al., 2025).

2.4. NDVI and NDWI computation

Vegetation and water indices were computed from Sentinel-2 surface reflectance using standard formulations (Fu et al., 2024; McFeeters, 1996):

$$NDVI = \frac{NIR - Red}{NIR + Red}, \quad NDWI = \frac{Green - NIR}{Green + NIR}$$

where: *NIR* – band B8; *Red* – band B4; *Green* – band B3.

NDVI was used to quantify vegetation greenness, biomass condition, and seasonal phenological behaviour (Barbosa et al., 2006; Bulcock & Jewitt, 2010; Kumari et al., 2021), while NDWI was employed to delineate surface water extent and monitor hydrological variability (Peng K. et al., 2025; Zhong et al., 2025).

2.5. Temporal smoothing and gap-filling of NDVI time series

To reduce cloud-induced noise and fill observational gaps in the NDVI time series, a moving-window temporal smoothing filter was applied to the monthly NDVI composites. The smoothed NDVI is:

$$NDVI_t^* = \frac{1}{2k+1} \sum_{i=-k}^{i=k} NDVI_{t+i}$$

Following sensitivity analysis, a smoothing window size of $k = 2$ was selected as the optimal balance between noise suppression and preservation of seasonal vegetation signals (Fu et al., 2024; Kumari et al., 2021). This approach significantly improves temporal continuity and trend detectability in cloud-prone monsoon environments.

2.6. Machine-learning-based LULC classification

Supervised LULC classification was performed using three widely adopted machine-learning classifiers implemented within GEE: Random Forest (RF), Support Vector Machine (SVM), and Classification and Regression Tree (CART).

2.6.1. Training data and LULC classes

A stratified random sampling approach was employed to generate training and validation samples for supervised land-use/land-cover (LULC) classification. A total of approximately 2,800 reference samples were collected across five dominant LULC classes, selected to reflect hydrologically and operationally relevant catchment characteristics influencing reservoir inflows and storage behaviour:

- water bodies;
- agricultural land;
- vegetation;
- built-up land;
- bare land.

Seventy percent of the samples were used for classifier training, while the remaining thirty percent were reserved for independent validation (Congalton & Green, 2019). The inclusion of agriculture and bare land as separate classes enabled improved discrimination of runoff-generating surfaces and sediment-prone zones, which are critical for assessing catchment-induced stress on reservoir operation.

2.6.2. Random forest (RF)

RF is an ensemble learning classifier that constructs multiple decision trees and aggregates their predictions through majority voting (Breiman, 2001). The RF model was parameterised with:

- number of trees (nTree) = 100;
- variables per split = $\sqrt{p}$;
- bootstrap aggregation enabled.

Feature importance was evaluated using the mean decrease in the Gini index (Belgiu & Drăguț, 2016).

Random forest was selected as the primary classification approach in this study because of its strong performance in heterogeneous landscapes and its robustness to the spectral variability, noisy training samples, and non-linear class boundaries commonly observed in semi-arid environments. Compared with individual decision-tree approaches, RF reduces overfitting through ensemble learning and generally provides higher classification stability and accuracy for multi-temporal remote-sensing applications. Preliminary comparison with the SVM and CART classifiers further confirmed that RF consistently achieved superior overall accuracy and kappa performance across all study years, supporting its suitability for operational decision-support applications within the Google Earth Engine platform.

2.6.3. Support vector machine (SVM)

The SVM classifier was implemented using a radial basis function (RBF) kernel. Hyperparameters were optimised using grid-search cross-validation with:

- regularisation parameter: $C = 10$;
- kernel width: $\gamma = 0.1$.

SVM is particularly effective in high-dimensional feature spaces and for non-linear class boundaries (Huang et al., 2002; Pande et al., 2024).

2.6.4. Classification and regression tree (CART)

The CART classifier was implemented using the Gini impurity criterion with the following parameters:

- maximum tree depth: 20;
- minimum leaf node size: 5.

CART is computationally efficient but sensitive to variations in the training sample (Jin et al., 2018; Purwanto et al., 2023).

The selected LULC classes were intentionally limited to hydrologically meaningful categories to ensure robustness and operational interpretability of catchment-scale indicators for reservoir management. The selected classes were designed to represent the dominant land-surface characteristics controlling the hydrological response within the Pakhal Lake catchment. The water bodies class directly reflects reservoir storage conditions, while the vegetation and agricultural land classes represent relatively permeable, hydrologically moderating surfaces that influence infiltration, evapotranspiration, and runoff attenuation. In contrast, the built-up land and bare land classes represent hydrologically responsive surfaces associated with increased runoff generation, reduced infiltration, increased erosion susceptibility, and sediment mobilisation. The selected classification scheme, therefore, captures the principal catchment processes influencing reservoir inflow variability, flood dynamics, and long-term storage stability. Restricting the analysis to five major classes also reduced spectral confusion and improved classification consistency in the heterogeneous semi-arid environment.

2.7. Sentinel-1 SAR-based flood inundation mapping

Flood inundation was detected using Sentinel-1 VH-polarised SAR imagery due to its high sensitivity to smooth open-water surfaces (Lang et al., 2024; Narin et al., 2025). A refined Lee speckle filter with a 5 × 5 kernel was applied to suppress multiplicative noise while preserving edge information.

Flooded pixels were identified using a backscatter ratio-based thresholding approach:

$$\Delta VH = \frac{VH_{post}}{VH_{pre}}$$

Pixels with $\Delta VH > 1.25$ were classified as flooded. The threshold was selected through histogram-based class separability analysis and optical–SAR cross-validation (Narin et al., 2025; Peng K. et al., 2025). Permanent water bodies, steep slopes (>15°), and isolated noise pixels were removed using DEM-based masking and morphological filtering.

2.8. Post-classification change detection

Inter-annual LULC change was quantified using post-classification comparison, which minimises radiometric inconsistencies and sensor-related bias (Asokan & Anitha, 2019).

Change transition matrices were generated to quantify:

- water → bare land;
- vegetation → built-up land;
- water → built-up land.

All LULC maps were spatially clipped to the Pakhal Lake catchment boundary prior to area calculation, and class-wise areas were computed using pixel-area weighting and converted to hectares to ensure physical consistency across years.

2.9. Accuracy assessment and uncertainty analysis

Classification performance was evaluated using the standard confusion matrix-based accuracy metrics:

- overall accuracy (OA);
- producer's accuracy (PA);
- user's accuracy (UA);
- F1-score;
- Kappa coefficient (κ).

Kappa uncertainty was estimated based on large-sample variance theory (Fleiss et al., 1969). Quantity and allocation disagreement were quantified following the method defined by Pontius and Millones (2011). Model stability and generalisation capability were evaluated using five-fold cross-validation (Congalton & Green, 2019).

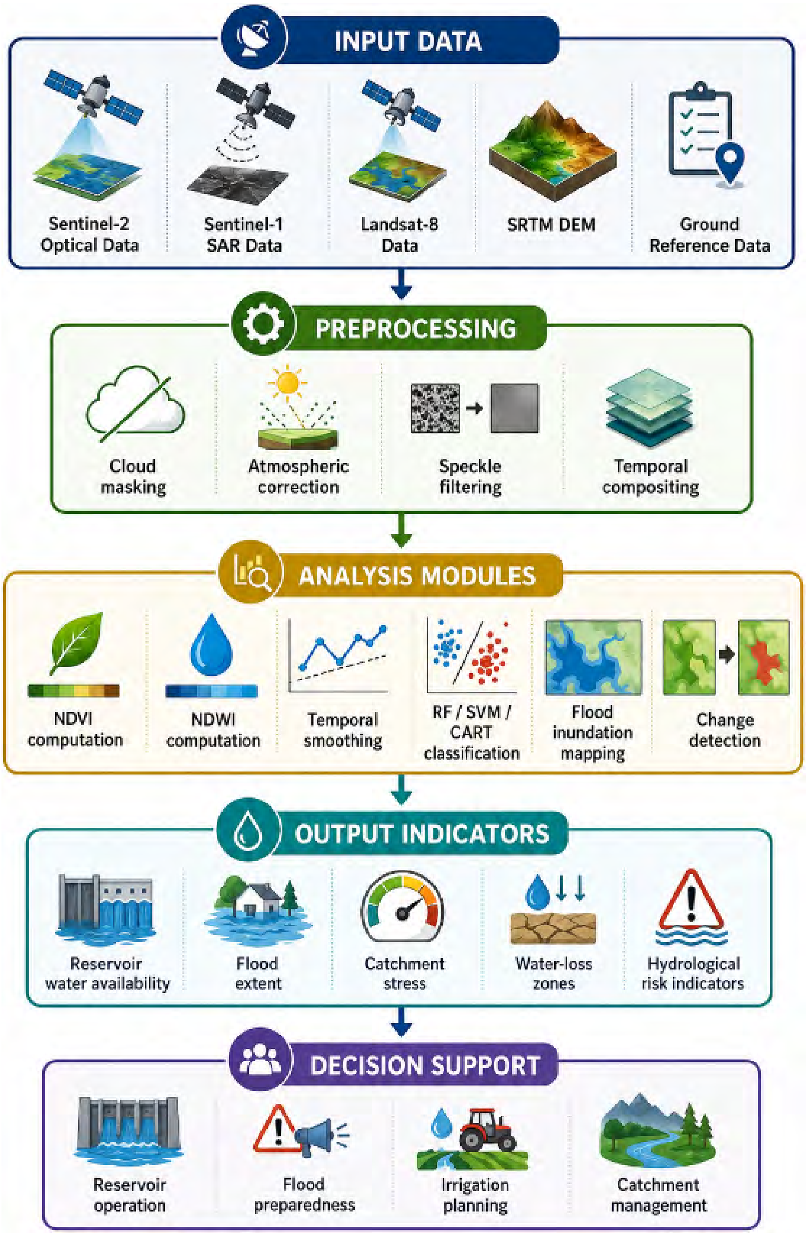

Fig. 2. Operational satellite-enabled decision-support framework for reservoir monitoring and catchment stress assessment

3. Results

3.1. Seasonal and interannual vegetation dynamics linked to reservoir storage (NDVI)

The Sentinel-2-derived NDVI time series for Pakhal Lake, from 2016 to 2021, exhibits pronounced seasonal and interannual variability (Fig. 3). NDVI values ranged from approximately 0.10 to 0.52, with consistent annual maxima during the post-monsoon period (September–October) and minima during the late dry season (April–May). Similar seasonal vegetation responses to reservoir-controlled hydrology have been reported for semi-arid wetlands and inland water bodies (Aquino et al., 2024; Barbosa et al., 2006; Kumari et al., 2021).

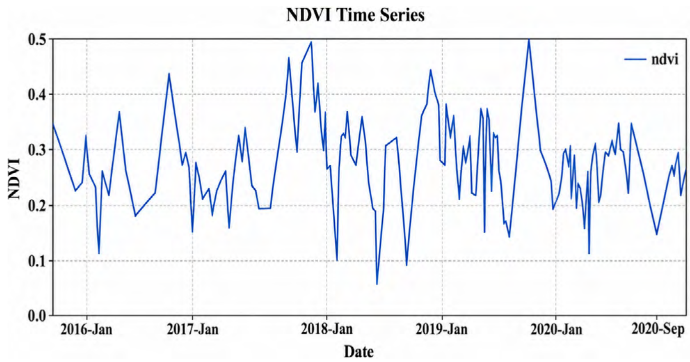

Fig. 3. Sentinel-2-derived NDVI time series over Pakhal Lake for the period 2016–2021

Interannual differences were observed in the NDVI time series. The year 2019 recorded the highest mean NDVI (~0.51), whereas 2017 and 2020 exhibited comparatively lower NDVI values (India Meteorological Department, 2020; Sheffield et al., 2012). These results confirm that vegetation dynamics within and around the reservoir are sensitive to variations in reservoir water availability.

3.2. Effect of temporal smoothing on NDVI time series

Application of the moving-window temporal smoothing filter (k = 2) substantially improved the continuity of the NDVI time series by suppressing cloud-related noise while preserving seasonal signals (Fig. 4). The smoothed NDVI profile retained its characteristic seasonal peaks and troughs, with values ranging between approximately 0.18 and 0.51, and a mean of approximately 0.38.

The smoothed NDVI time series exhibited reduced short-term variability while preserving seasonal peaks and troughs (Kumari et al., 2021; Fu et al., 2024).

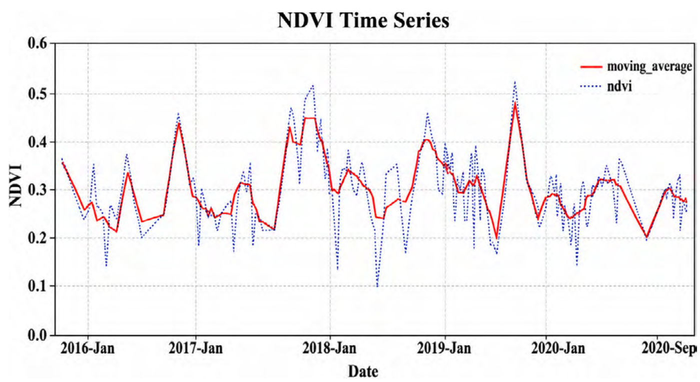

Fig. 4. Effect of moving-window temporal smoothing (k = 2) on Sentinel-2 NDVI time series over Pakhal Lake

3.3. Catchment land-use/land-cover changes

RF-based land-use/land-cover (LULC) classification identified five dominant classes: agriculture, water bodies, built-up land, vegetation, and bare land (Fig. 5). Classification performance was high, with overall accuracies ranging from 93% to 97% and kappa coefficients between 0.94 and 0.98 across all years (Tab. 2), comparable to similar applications in heterogeneous semi-arid landscapes (Belgiu & Drăguţ, 2016; Jin et al., 2018).

Tab. 2. Comparative classification accuracy of machine-learning classifiers for land-use/land-cover mapping of the Pakhal Lake catchment (2018–2021)

Year	Classifier	Overall accuracy (OA) [%]	Kappa coefficient (κ)
2018	RF	93.4	0.94
	SVM	92.1	0.91
	CART	88.6	0.86
2019	RF	95.2	0.96
	SVM	93.4	0.92
	CART	89.8	0.87
2020	RF	96.8	0.97
	SVM	94.6	0.94
	CART	90.5	0.88
2021	RF	97.1	0.98
	SVM	95.0	0.95
	CART	91.2	0.89

Quantitative analysis of clipped catchment-scale LULC maps indicates a substantial increase in anthropogenically modified surfaces, including built-up and peri-urban areas, from approximately 1,980 ha in 2018 to 3,840 ha in 2021. This increase likely reflects a combination of settlement expansion, infrastructure growth, exposed compacted surfaces, and transitional land-cover conditions within the catchment. Similarly, bare land increased from approximately 5,420 ha to 6,220 ha over the same period (Tab. 3), likely associated with exposed sediment surfaces, seasonally dry, sparsely vegetated areas, fallow agricultural land, and progressive land degradation. While the random forest classifier achieved high overall accuracy, some spectral overlap between the built-up land and bare land classes in semi-arid environments may contribute to uncertainty in the magnitude of change.

Tab. 3. Year-wise land-use/land-cover (LULC) area statistics for the Pakhal Lake catchment derived from Sentinel-2 imagery (2018–2021) [ha]

Year	Agriculture	Water body	Built-up land	Vegetation	Bare land	Total
2018	7,950	1,420	1,980	10,230	5,420	27,000
2019	8,420	960	2,110	9,430	6,080	27,000
2020	8,610	1,870	2,320	9,010	5,190	27,000
2021	6,940	1,790	3,840	8,210	6,220	27,000

Fig. 5 presents the Sentinel-2-derived representative land-use/land-cover (LULC) map of the Pakhal Lake catchment. Five dominant classes – agriculture, water bodies, vegetation, built-up land, and bare land – were identified using the random forest classifier, which consistently achieved high classification accuracy (Tab. 2). The maps indicate a progressive expansion of built-up and bare land, particularly along transportation corridors and near reservoir inflow zones, accompanied by a relative reduction in vegetation and agricultural cover.

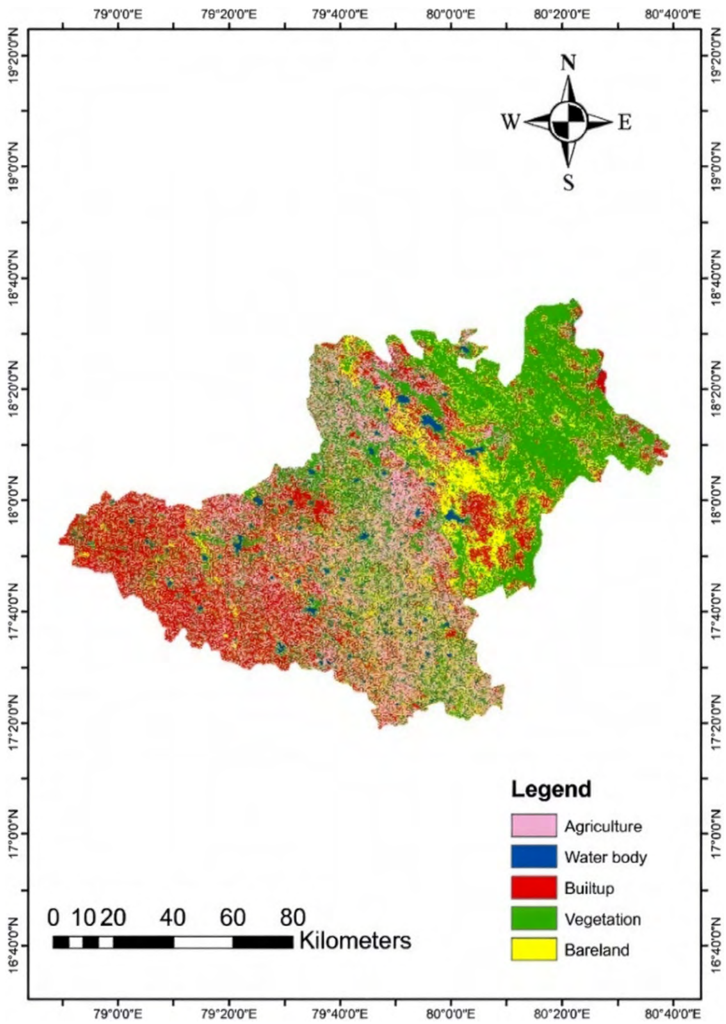

Fig. 5. Sentinel-2-derived representative land-use/land-cover (LULC) classification of the Pakhal Lake catchment

3.4. Interannual water-body contraction and spatial water loss patterns (2019–2020)

Interannual comparison of the Sentinel-2-derived water-body extent between 2019 and 2020 reveals substantial spatial contraction of the reservoir surface area (Fig. 6). The reduction in water extent is particularly evident along the peripheral shallow zones and inflow margins, indicating the progressive exposure of previously inundated areas. The observed contraction patterns likely reflect the combined influence of seasonal abstraction, evaporation losses, interannual variability in monsoon recharge, and catchment-scale hydrological changes.

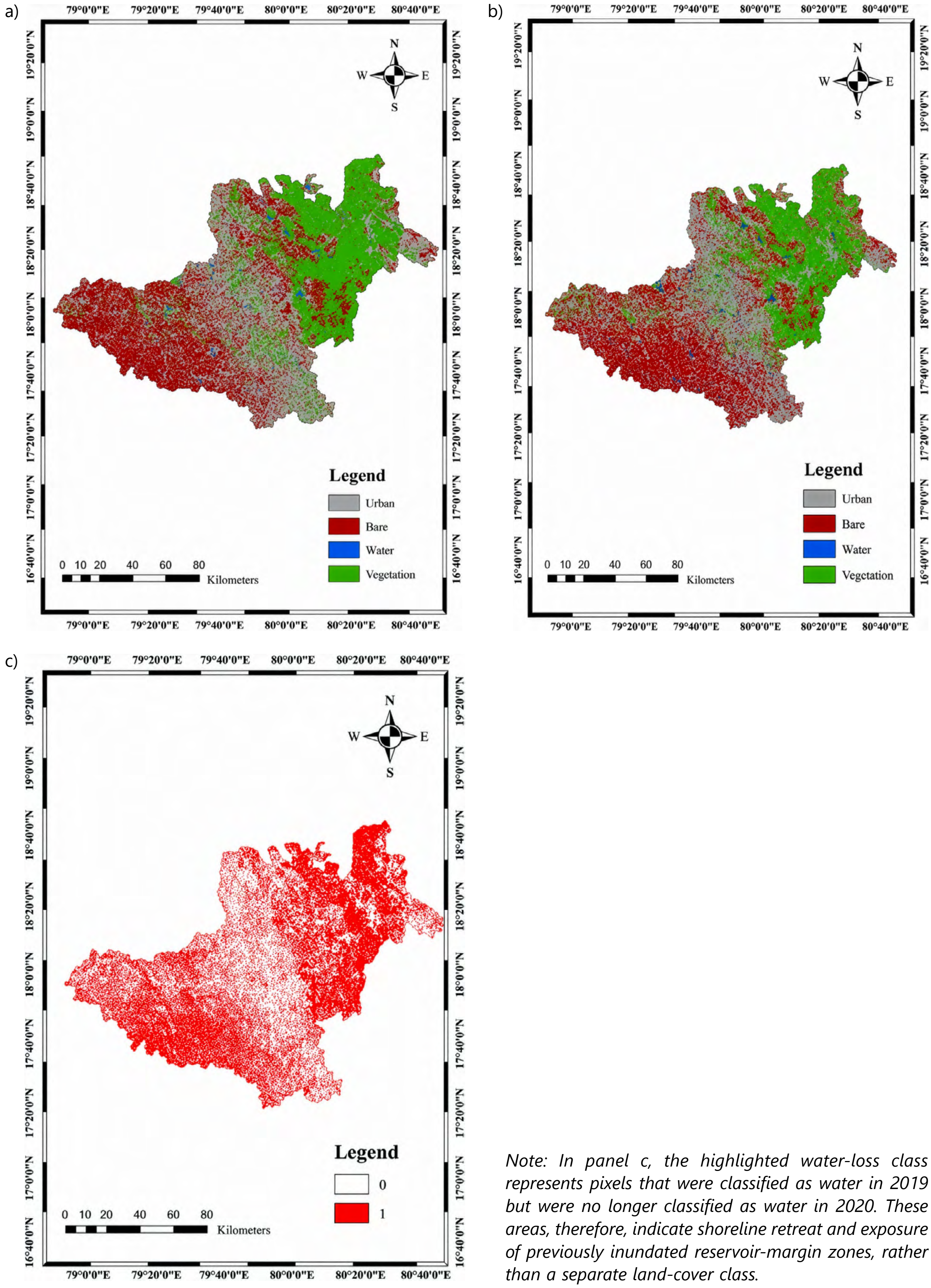

Note: In panel c, the highlighted water-loss class represents pixels that were classified as water in 2019 but were no longer classified as water in 2020. These areas, therefore, indicate shoreline retreat and exposure of previously inundated reservoir-margin zones, rather than a separate land-cover class.

Fig. 6. Water-body extent derived from Sentinel-2 imagery: a) for 2019; b) for 2020; c) spatial distribution of water loss between 2019 and 2020

The spatial water-loss map (Fig. 6c) highlights non-uniform contraction, with greater losses concentrated in low-slope zones adjacent to agricultural and bare-land regions. This pattern suggests that marginal reservoir storage is sensitive to interannual variability in monsoon inflows and dry-season abstraction. Similar spatial contraction patterns have been reported for semi-arid reservoirs experiencing fluctuating hydrological inputs (Aquino et al., 2024; Mohanty et al., 2020).

3.5. Seasonal reservoir water-extent variability (NDWI)

NDWI-derived maps for 2018 reveal pronounced seasonal variability in the reservoir surface-water extent (Fig. 7). During the monsoon season (June–October), positive NDWI values indicate extensive surface-water coverage, whereas the dry season (January–April) is characterised by substantial contraction of the reservoir water body.

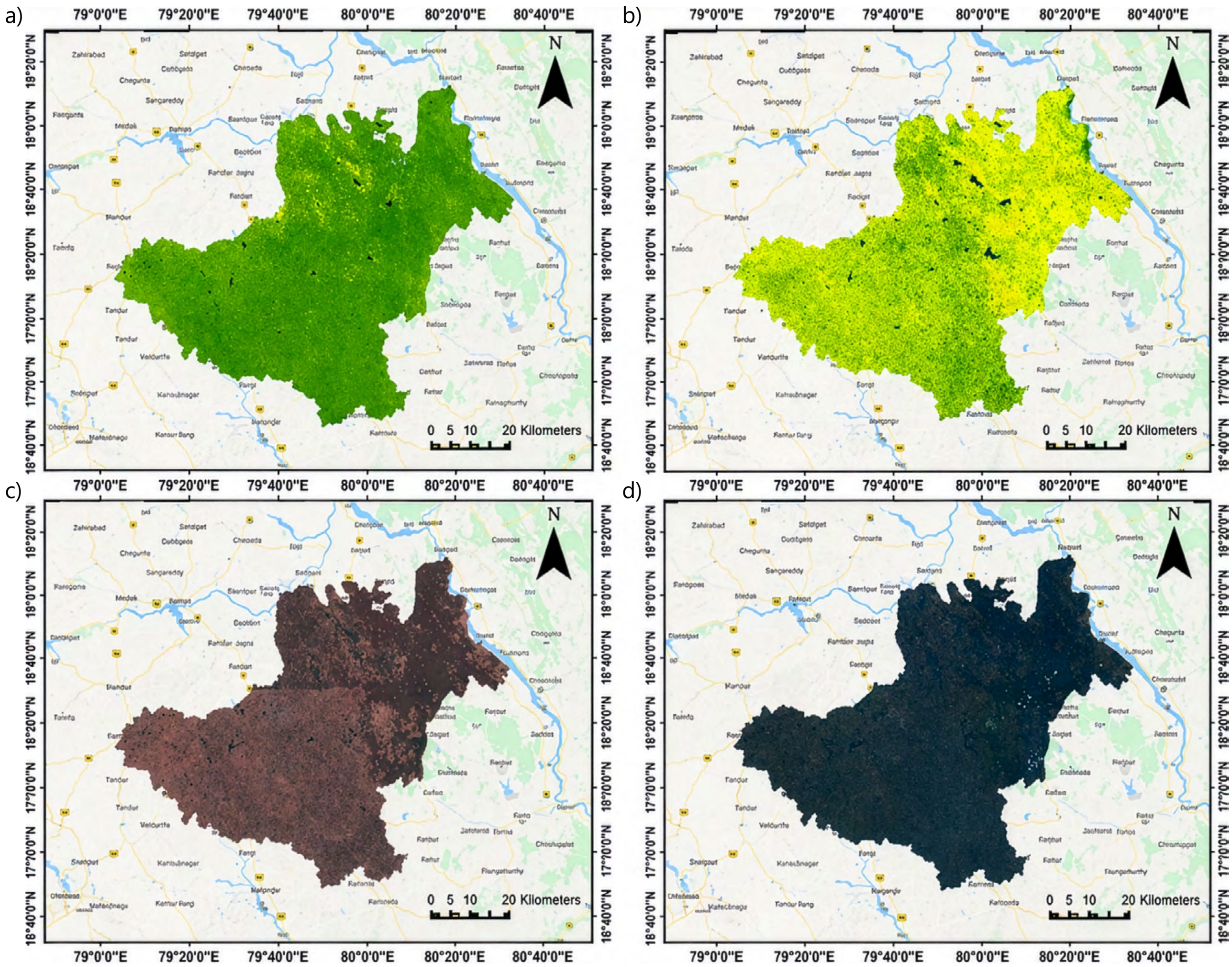

Fig. 7. Seasonal NDWI-derived surface-water extent over Pakhal Lake for 2018 showing classified NDWI maps for (a) dry season and (b) wet season, and corresponding true-colour Sentinel-2 composites for (c) dry season and (d) wet season

This seasonal contrast reflects the dominance of monsoon-driven inflows, followed by dry-season storage depletion, consistent with NDWI-based reservoir assessments reported in earlier studies (McFeeters, 1996; Peng X. et al., 2025).

3.6. Flood inundation extent during extreme monsoon conditions

Sentinel-1 SAR analysis of the extreme monsoon event in 2018 indicates that flood inundation expanded the reservoir surface area by approximately 28% relative to pre-monsoon conditions (Fig. 8). Flooded zones were predominantly located along low-lying reservoir margins and inflow channels.

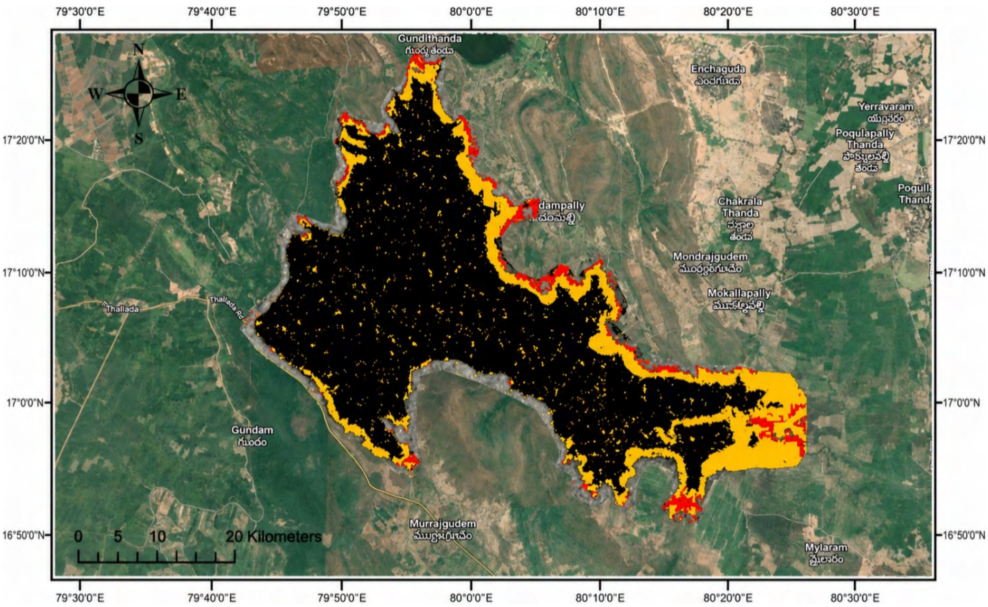

Fig. 8. Sentinel-1 SAR-derived flood inundation extent and pre-flood water extent during the 2018 monsoon

The SAR-derived flood extent demonstrates the radar imagery's capability to reliably capture inundation patterns under persistent cloud cover, in agreement with previous SAR-based flood-mapping studies in monsoon-affected regions (Lang et al., 2024; Narin et al., 2025).

3.7. Performance of machine-learning classifiers

A comparative assessment of CART, SVM, and RF classifiers reveals that RF consistently outperforms the other algorithms, achieving overall accuracies ranging from 93.4% to 97.1% and kappa coefficients from 0.94 to 0.98 (Tab. 2). SVM achieved slightly lower accuracies, while CART exhibited the lowest performance across all years.

4. Discussion

4.1. Vegetation dynamics as indicators of reservoir water availability

The seasonal NDVI patterns observed in this study indicate a strong linkage between vegetation greenness and reservoir water availability. Peak NDVI during the post-monsoon period reflects enhanced soil moisture and sustained reservoir storage, while dry-season declines correspond to reservoir drawdown and increased evapotranspiration losses. Similar NDVI–hydrology relationships have been reported for semi-arid reservoirs and wetlands (Barbosa et al., 2006; Liu et al., 2024; Peng K. et al., 2025).

From an operational standpoint, NDVI time series provide a cost-effective proxy for assessing seasonal water sufficiency, particularly in regions where continuous in-situ storage monitoring is limited (Mohanty et al., 2020).

An important advantage of the proposed framework is its ability to capture not only the presence of hydrological change but also its spatial extent, persistence, and temporal evolution. This enhances its applicability for operational reservoir monitoring, especially in semi-arid regions where rapid shifts between flood and water-stress conditions can occur within short seasonal timescales.

4.2. Operational importance of temporal smoothing

Temporal smoothing proved essential for extracting reliable NDVI signals in cloud-affected monsoon environments. Without smoothing, short-term artefacts could be misinterpreted as vegetation stress or recovery, potentially leading to erroneous assessments of reservoir performance. Previous studies have similarly highlighted the importance of smoothing techniques for operational vegetation monitoring (Kumari et al., 2021; Peng K. et al., 2025). From a decision-support perspective, temporal smoothing improves the reliability of satellite-derived indicators used for reservoir management by reducing the false anomaly detection caused by cloud contamination and atmospheric variability. This is particularly important in monsoon-dominated regions where operational decisions may otherwise be influenced by short-term observational artefacts.

4.3. Catchment land-use change and hydrological stress

The land-use/land-cover patterns shown in Fig. 4 have direct implications for runoff generation, sediment transport, and operational stress on the Pakhal Lake reservoir. The observed expansion of built-up land and bare-land surfaces within the catchment represents a transition towards more hydrologically responsive terrain, characterised by reduced infiltration capacity and increased surface runoff during monsoon rainfall events. Such changes are known to amplify peak inflows to reservoirs, shortening runoff concentration times and increasing pressure on spillway operations during high-intensity rainfall (Aquino et al., 2024; Shekar & Mathew, 2023).

The observed increase in bare-land surfaces, including exposed soils, fallow agricultural fields, and sediment-exposed reservoir margins, is operationally significant because such areas are highly susceptible to erosion during monsoon storms. Increased sediment mobilisation from these areas can accelerate reservoir siltation, progressively reducing effective storage capacity and altering stage–storage relationships. This sediment-induced loss of usable storage directly affects dry-season water availability, irrigation reliability, and long-term reservoir sustainability, especially in semi-arid regions where storage buffers are limited.

The spatial distribution of built-up land in proximity to inflow channels further exacerbates these challenges. Impervious surfaces associated with urban and peri-urban development generate rapid runoff pulses that increase inflow variability and reduce the predictability of reservoir response. For reservoir operators, this translates into narrower operational windows for flood attenuation and greater uncertainty in balancing flood control and water-supply objectives during extreme monsoon events.

Conversely, areas classified as vegetation and agricultural land play a moderating role by enhancing infiltration, attenuating runoff, and reducing sediment yield. The observed reduction and fragmentation of these classes therefore represent a loss of natural buffering capacity within the catchment. This shift increases the likelihood that identical rainfall events will produce progressively higher inflows and sediment loads over time, even in the absence of changes in rainfall magnitude.

From a water-resources and industry standpoint, the LULC trends identified in Fig. 4 provide actionable intelligence for reservoir management. Zones exhibiting rapid built-up and bare-land expansion can be prioritised for catchment-level interventions such as erosion-control measures, afforestation, buffer-zone enforcement, and land-use regulation. Incorporating these spatial indicators into reservoir operation strategies enables more informed flood preparedness planning, sediment management, and long-term storage optimisation.

Overall, the integration of machine-learning-based LULC analysis with reservoir water-extent and flood-inundation monitoring transforms Fig. 4 from a descriptive land-cover map into an operational diagnostic tool, directly supporting decision-making for sustainable reservoir operation under increasing climatic and anthropogenic pressure.

4.4. Significance of interannual water-body contraction for reservoir reliability

The interannual water-body contraction observed between 2019 and 2020 (Fig. 6) reflects short-term hydrological stress superimposed on long-term pressures from the catchment and climate (Dixon et al., 2016). The concentration of water loss along shallow reservoir margins suggests adequate storage, but also increased vulnerability of fringe zones to evaporation losses and sediment exposure.

From a reservoir-operation perspective, such spatially uneven contraction has direct implications for storage reliability and water allocation. Marginal water losses reduce usable storage earlier in the dry season, potentially limiting irrigation supply and increasing dependence on groundwater abstraction. Comparable interannual contraction behaviour has been documented in other semi-arid reservoirs subjected to rainfall variability and catchment disturbance (Aquino et al., 2024; Shekar & Mathew, 2023).

The observed contraction between 2019 and 2020 should also be interpreted within the context of interannual hydro-meteorological variability. The extreme monsoon conditions recorded across parts of southern India in 2018 likely contributed to enhanced reservoir recharge, temporary floodplain expansion, and elevated post-monsoon storage. Consequently, the apparent water-loss patterns observed during 2019–2020 may partly reflect a transition from anomalously wet antecedent conditions towards more typical seasonal storage behaviour. This highlights the importance of interpreting satellite-derived reservoir dynamics in conjunction with regional rainfall variability, monsoon intensity, evaporation losses, and seasonal water abstraction.

Importantly, the spatial water-loss patterns identified in Fig. 6c provide actionable information for reservoir managers, enabling them to identify high-risk zones where sedimentation control, desilting, or buffer-zone protection measures could enhance long-term storage stability.

4.5. Flood expansion and reservoir safety implications

The 28% flood-driven expansion observed during the 2018 extreme monsoon suggests that the reservoir operated close to its hydrological capacity threshold.

Such conditions have direct implications for spillway operation, dam safety, and downstream flood risk. SAR-based flood mapping provides a reliable tool for near-real-time flood preparedness and emergency response under cloud-covered conditions (Lang et al., 2024; Narin et al., 2025). The integration of SAR-derived flood extent with reservoir monitoring frameworks also enables improved identification of vulnerable inundation zones and supports adaptive reservoir-release strategies during extreme rainfall events.

4.6. Reliability of machine-learning approaches for decision support

The superior performance of the RF classifier confirms its suitability for operational catchment monitoring in heterogeneous semi-arid landscapes. High classification reliability is critical for decision-support applications, as inaccuracies in land-cover mapping can propagate uncertainty into runoff estimation and flood-risk assessments (Belgiu & Drăguț, 2016). The operational efficiency of random forest within cloud-based platforms such as Google Earth Engine further enhances its applicability for large-scale and near-real-time reservoir monitoring programmes.

4.7. Integrated climatic and anthropogenic controls on reservoir dynamics

The combined evidence from vegetation indices, water extent analysis, flood mapping, and LULC change indicates that the interaction of climatic variability and anthropogenic pressures increasingly influences Pakhal Lake. Intensified monsoon extremes exacerbate flood hazards, while land-use transformation accelerates the depletion of seasonal storage. Similar coupled impacts have been reported for semi-arid reservoirs globally (Jain et al., 2020; Sheffield et al., 2012).

4.8. Implications for water resources and industry

By translating multi-sensor satellite observations into operationally relevant indicators, the proposed framework enables proactive reservoir management, enhanced flood preparedness, and informed irrigation planning. Its scalability and low data requirements make it particularly suitable for water resources agencies operating in data-scarce, semi-arid regions. The framework also supports long-term climate adaptation planning by enabling continuous assessment of hydrological stress, storage variability, and catchment transformation under evolving climatic and land-use conditions.

5. Conclusions

This study demonstrates the practical value of integrating multisensor satellite observations and machine learning analytics into an operational decision-support framework for reservoir management in semi-arid regions.

Based on the results, the following key conclusions are drawn:

- Operational monitoring of reservoir water availability:

  Temporally smoothed NDVI and NDWI time series provide reliable and spatially explicit indicators of seasonal and interannual reservoir water availability. Beyond identifying general vegetation–water relationships, the integrated framework enables continuous monitoring of the scale, spatial distribution, and temporal dynamics of hydrological change across the reservoir and its catchment. This capability is particularly important for detecting progressive storage contraction, flood expansion, vegetation stress, and emerging catchment disturbances under changing climatic and anthropogenic pressures. The framework demonstrated strong performance in capturing both gradual and abrupt hydrological transitions at fine spatial (10 m for Sentinel-2, 30 m for Landsat) and temporal (5-day revisit) resolutions. The 28% flood-area expansion detected during the 2018 extreme monsoon, together with the spatially resolved water-body contraction mapped between 2019 and 2020, illustrates the tool's capacity to resolve changes across scales ranging from local shoreline retreat to catchment-wide inundation. Temporal smoothing of the NDVI time series further ensured that seasonal vegetation dynamics were recovered with high fidelity even under persistent monsoon cloud cover, yielding a mean smoothed NDVI of ~0.38 with clear post-monsoon peaks (~0.51) and dry-season minima (~0.18). These metrics confirm that the integrated approach not only detects change but quantifies its magnitude, spatial extent, and rate with sufficient precision to inform operational decisions.

- Flood preparedness and capacity stress assessment:

  Sentinel-1 SAR-based flood mapping reliably captured extreme monsoon inundation under persistent cloud cover, revealing flood-driven expansion of approximately 28% of the reservoir area. This information is directly applicable to spillway operation planning, dam safety assessment, and downstream flood risk mitigation.

- Catchment-induced hydrological stress detection:

  Machine-learning-based land-use analysis identified the rapid expansion of built-up and bare land within the catchment, indicating an increasing runoff potential, sediment delivery, and long-term pressure on adequate reservoir storage capacity.

- Decision-support reliability using machine learning:

  Random forest consistently outperformed alternative classifiers, confirming its suitability for routine, operational catchment monitoring where classification reliability is essential for runoff estimation and flood-risk evaluation.

- Integrated climate–land-use impacts on reservoir performance:

  The combined analysis reveals that interacting hydro-climatic variability and anthropogenic catchment transformation are progressively shifting the reservoir towards a more operationally sensitive state, increasing both its flood vulnerability during monsoon seasons and water scarcity during dry periods.

- Scalability and applicability for water-resources agencies:

  The proposed framework is scalable, cost-effective, and transferable to other data-scarce, semi-arid reservoirs, offering water resources agencies a practical tool to transition from reactive to proactive reservoir operation, flood preparedness, and sustainable water governance (Convention on Wetlands, 2025).

Data availability statement

The Sentinel-1 and Sentinel-2 satellite datasets used in this study are freely available from the Copernicus Open Access Hub and were accessed via the Google Earth Engine (GEE) cloud-computing platform. Landsat-8 imagery is available from the United States Geological Survey (USGS) Earth Explorer. The SRTM digital elevation model (DEM) is available from the USGS data repository. Derived products generated in this study are available from the corresponding author upon reasonable request.

Code availability statement

All image preprocessing, index computation, machine-learning classification, and post-classification change detection were implemented using custom scripts developed within the Google Earth Engine (GEE) JavaScript API environment. The scripts used in this study can be provided by the corresponding author upon reasonable request for academic and research purposes.

Conflicts of interest

The authors declare no conflict of interest.

Abbreviations

Abbreviation	Full form
CART	classification and regression tree
DEM	digital elevation model
GEE	Google Earth Engine
GRD	ground range detected
IW	interferometric wide
κ	Kappa coefficient
LULC	land-use/land-cover
NDVI	normalised difference vegetation index
NDWI	normalised difference water index
OA	overall accuracy
OLI	operational land imager
PA	producer's accuracy
RBF	radial basis function
RF	random forest
SAR	synthetic aperture radar
SRTM	shuttle radar topography mission
SVM	support vector machine
SWIR	shortwave infrared
TOA	top of atmosphere
UA	user's accuracy
UTM	universal transverse mercator
VH	vertical–horizontal polarisation
VIS	visible
WGS 84	World Geodetic System 1984

References

Aquino, D. S., Gavier-Pizarro, G., Rescia, A. J., & Quintana, R. D. (2024). Wetland responses to non-stationary hydro-climatic dynamics in the context of land cover and land use change. *Remote Sensing Applications: Society and Environment*, *34*, Article 101156. https://doi.org/10.1016/j.rsase.2024.101156

Asokan, A., & Anitha, J. (2019). Change detection techniques for remote sensing applications: A survey. *Earth Science Informatics*, *12*, 143–160. https://doi.org/10.1007/s12145-019-00380-5

Barbosa, H. A., Huete, A. R., & Baethgen, W. E. (2006). A 20-year study of NDVI variability over the Northeast region of Brazil. *Journal of Arid Environments*, *67*(2), 288–307. https://doi.org/10.1016/j.jaridenv.2006.02.022

Bassi, N., Kumar, M. D., Sharma, A., & Pardha-Saradhi, P. (2014). Status of wetlands in India: A review of extent, ecosystem benefits, threats and management strategies. *Environmental Management*, *2*, 1–19. https://doi.org/10.1016/j.ejrh.2014.07.001

Belgiu, M., & Drăguţ, L. (2016). Random forest in remote sensing: A review of applications and future directions. *ISPRS Journal of Photogrammetry and Remote Sensing*, *114*, 24–31. https://doi.org/10.1016/j.isprsjprs.2016.01.011

Breiman, L. (2001). Random forests. *Machine Learning*, *45*(1), 5–32. https://doi.org/10.1023/A:1010933404324

Bulcock, H. H., & Jewitt, G. P. W. (2010). Spatial mapping of leaf area index using hyperspectral remote sensing for hydrological applications with a particular focus on canopy interception. *Hydrology and Earth System Sciences*, *14*(2), 383–392. https://doi.org/10.5194/hess-14-383-2010

Congalton, R. G., & Green, K. (2019). *Assessing the Accuracy of Remotely Sensed Data: Principles and Practices* (3rd ed.). CRC Press. https://doi.org/10.1201/9780429052729

Convention on Wetlands (2025). *Global Wetland Outlook 2025: Valuing, conserving, restoring and financing wetlands*. Secretariat of the Convention on Wetlands. https://doi.org/10.69556/GWO-2025-eng

Davidson, N. C. (2014). How much wetland has the world lost? Long-term and recent trends in global wetland area. *Marine and Freshwater Research*, *65*(10), 934–941. https://doi.org/10.1071/MF14173

Dixon, M. J. R., Loh, J., Davidson, N. C., Beltrame, C., Freeman, R., & Walpole, M. (2016). Tracking global change in ecosystem area: The Wetland Extent Trends index. *Biological Conservation*, *193*, 27–35. https://doi.org/10.1016/j.biocon.2015.10.023

Fu, Y., Zhu, Z., Liu, L., Zhan, W., He, T., Shen, H., Zhao, J., Liu, Y., Zhang, H., Liu, Z., Xue, Y., & Ao, Z. (2024). Remote sensing time series analysis: A review of data and applications. *Journal of Remote Sensing*, *4*, Article 0285. https://doi.org/10.34133/remotesensing.0285

Gorelick, N., Hancher, M., Dixon, M., Ilyushchenko, S., Thau, D., & Moore, R. (2017). Google Earth Engine: Planetary-scale geospatial analysis for everyone. *Remote Sensing of Environment*, *202*, 18–27. https://doi.org/10.1016/j.rse.2017.06.031

Hu, S., Niu, Z., Chen, Y., Li, L., & Zhang, H. (2017). Global wetlands: Potential distribution, wetland loss, and status. *Science of The Total Environment*, *586*, 319–327. https://doi.org/10.1016/j.scitotenv.2017.02.001

Huang, C., Davis, L. S., & Townshend, J. R. G. (2002). An assessment of support vector machines for land-cover classification. *International Journal of Remote Sensing*, *23*(4), 725–749. https://doi.org/10.1080/01431160110040323

India Meteorological Department. (2020). *Climatological normals and rainfall information for Telangana*. Ministry of Earth Sciences, Government of India. https://mausam.imd.gov.in/

Jin, Y., Liu, X., Chen, Y., & Liang, X. (2018). Land-cover mapping using random forest classification and NDVI time series and texture. *International Journal of Remote Sensing*, *39*(23), 8703–8723. https://doi.org/10.1080/01431161.2018.1490976

Kumari, N., Srivastava, A., & Dumka, U. C. (2021). A long-term spatiotemporal analysis of vegetation greenness over the Himalayan Region using Google Earth Engine. *Climate*, *9*(7), Article 109. https://doi.org/10.3390/cli9070109

Lang, F., Zhu, Y., Zhao, J., Hu, X., Shi, H., Zheng, N., & Zha, J. (2024). Flood mapping of synthetic aperture radar (SAR) imagery based on semi-automatic thresholding and change detection. *Remote Sensing*, *16*(15), Article 2763. https://doi.org/10.3390/rs16152763

Liu, W. (2024). The response of NDVI to drought at different temporal scales in the Yellow River Basin from 2003 to 2020. *Water*, *16*(17), Article 2416. https://doi.org/10.3390/w16172416

Louis, J., Debaecker, V., Pflug, B., Main-Knorn, M., Bieniarz, J., Mueller-Wilm, U., Cadau, E., & Gascon, F. (2016). Sentinel-2 Sen2Cor: L2A processor for users. In *'Living Planet Symposium 2016', Prague, Czech Republic, 9–13 May 2016 (ESA SP-740, August 2016)*. https://elib.dlr.de/107381/

McFeeters, S. K. (1996). The use of the normalised difference water index (NDWI) in the delineation of open water features. *International Journal of Remote Sensing*, *17*(7), 1425–1432. https://doi.org/10.1080/01431169608948714

Merchant, M., Brisco, B., Mahdianpari, M., Bourgeau-Chavez, L., Murnaghan, K., DeVries, B., & Berg, A. (2023). Leveraging Google Earth Engine cloud computing for large-scale Arctic wetland mapping. *International Journal of Applied Earth Observation and Geoinformation*, *125*, Article 103589. https://doi.org/10.1016/j.jag.2023.103589

Mitsch, W. J., Gosselink, J. G., Anderson, C. J., & Fennessy, M. S. (2023). *Wetlands* (6th ed.). John Wiley & Sons. https://www.wiley.com/Wetlands%2C+6th+Edition-p-9781119826958

Mohanty, M., Mudgil, S., & Karmakar, S. (2020). Flood management in India: A focused review on the current status and future challenges. *International Journal of Disaster Risk Reduction*, *49*, Article 101660. https://doi.org/10.1016/j.ijdrr.2020.101660

Narin, O. G., Sekertekin, A., Bayik, C., Balcik, F. B., Arıkan, M., Sanli, F. B., & Abdikan, S. (2025). Multi-sensor flood mapping in urban and agricultural landscapes of the Netherlands using SAR and optical data with random forest classifier. *Remote Sensing*, *17*(15), Article 2712. https://doi.org/10.3390/rs17152712

Pan, X., Wang, Z., Feng, G., Wang, S., & Samiappan, S. (2025). Automated mapping of land cover in Google Earth Engine platform using multispectral Sentinel-2 and MODIS image products. *PLoS ONE*, *20*(4), Article e0312585. https://doi.org/10.1371/journal.pone.0312585

Pande, C. B., Srivastava, A., Moharir, K. N., Radwan, N., Sidek, L. M., Alshehri, F., Pal, S. C., Tolche, A. D., & Zhran, M. (2024). Characterizing land use/land cover change dynamics by an enhanced random forest machine learning model: A Google Earth Engine implementation. *Environmental Sciences Europe*, *36*, Article 84. https://doi.org/10.1186/s12302-024-00901-0

Peng, K., Tang, X., Li, R., Wang, D., & Hu, Y. (2025). From flood to drought: Integrating water level magnitude and timing to predict floodplain vegetation dynamics in Poyang Lake. *Ecological Indicators*, *177*, Article 113798. https://doi.org/10.1016/j.ecolind.2025.113798

Peng, X., Chen, S., Miao, Z., Xu, Y., Ye, M., & Lu, P. (2025). Automatic flood monitoring with SAR and optical data using Google Earth Engine. *Water*, *17*(2), Article 177. https://doi.org/10.3390/w17020177

Priyadarshini, P. (2025). Resilience in wetland conservation: A review on comparative study of high-altitude and low-altitude wetlands in India. *Journal of Applied and Natural Science*, *17*(3), 1110–1120. https://doi.org/10.31018/jans.v17i3.6712

Purwanto, A. D., Wikantika, K., Deliar, A., & Darmawan, S. (2023). Decision tree and random forest classification algorithms for mangrove forest mapping in Sembilang National Park, Indonesia. *Remote Sensing*, *15*(1), Article 16. https://doi.org/10.3390/rs15010016

Sheffield, J., Wood, E. F., & Roderick, M. L. (2012). Little change in global drought over the past 60 years. *Nature*, *491*(7424), 435–438. https://doi.org/10.1038/nature11575

Shekar, P. R., & Mathew, A. (2023). Detection of land use/land cover changes in a watershed: A case study of the Murredu watershed in Telangana State, India. *Watershed Ecology and the Environment*, *5*, 46–55. https://doi.org/10.1016/j.wsee.2022.12.003

Zhong, A., Duan, X., Jin, W., & Zhang, M. (2025). Quantifying the relationship between the FPAR and vegetation index in marsh wetlands using a 3D radiative transfer model and satellite observations. *Remote Sensing*, *17*(18), Article 3223. https://doi.org/10.3390/rs17183223